Journal of Alloys and Compounds 693 (2017) 9–15

Contents lists available at ScienceDirect

Journal of Alloys and Compounds

journal homepage: http://www.elsevier.com/locate/jalcom

Effect of Cr_2O_3 addition on crystallization, microstructure and properties of $Li_2O–Al_2O_3–SiO_2$ glass-ceramics

Bo Li [a, b, c, *], Shanlin Wang [a], Yi Fang [a]

[a] School of Microelectronics and Solid-State Electronics, University of Electronic Science and Technology of China, Chengdu 610054, China
[b] State Key Laboratory of Electronic Thin Films and Integrated Devices, Chengdu 610054, China
[c] National Engineering Research Center of Electromagnetic Radiation Control Materials, Chengdu 610054, China

ARTICLE INFO

Article history:
Received 22 June 2016
Received in revised form
19 August 2016
Accepted 4 September 2016
Available online 6 September 2016

Keywords:
Glass-ceramic
LTCC
Coefficient of thermal expansion
Crystallization kinetics

ABSTRACT

A new glass-ceramic with high flexural strength and low thermal expansion based on $Li_2O–Al_2O_3–SiO_2$ (LAS) was prepared in this study. The effects of Cr_2O_3 addition on the crystallization, microstructure, flexural strength, thermal expansion, and electrical properties of LAS system were investigated. The crystallization kinetics based on DSC analysis was calculated using Kissinger and Ozawa methods, which showed that the activation energy E decreases from 158.5 to 149.3 kJ/mol, indicating that Cr_2O_3 is beneficial to the crystallization of LAS; the crystallization index n varies between 4.46 and 5.09, indicating that the crystallization manner is the volumetric crystallization. XRD analysis was estimated by the whole pattern fitting method, demonstrating that Cr_2O_3 addition could change the phase contents and promote the crystallinity. The crystallization of $CaMgSi_2O_6$ and Cr_2O_3 with higher CTE not only properly adjusted CTE for matching Si, but also dramatically improved the flexural strength for LAS glass-ceramic. Moreover, we provided a modified formula to calculate CTE of glass-ceramic in the acceptable range. LAS glass-ceramic with 3 wt% Cr_2O_3 sintered at 800 °C exhibited good properties: $\sigma = 208$ MPa, $\alpha = 2.64 \times 10^{-6}$/°C, $\varepsilon = 8.3$, $\tan\delta = 3.6 \times 10^{-3}$, $\rho = 8.82 \times 10^{12}$ Ω cm, indicating its suitability for LTCC application.

1. Introduction

In recent years, low temperature co-fired ceramic (LTCC) has been extensively employed in microelectronic packages for multilayer integrated circuits [1–4]. In order to meet high packing density and high frequency transportation, LTCC substrate materials should possess low thermal expansion ($<3 \times 10^{-6}$/°C), high mechanical strength (>150 MPa), and low dielectric constant (<9) [5–8].

Many glass-ceramic systems, such as $Li_2O–Al_2O_3–SiO_2$ [9], $MgO–Al_2O_3–SiO_2$ [10], $CaO–Al_2O_3–SiO_2$ [11], and $CaO–B_2O_3–SiO_2$ [12] have been developed. Further, the nucleating agents ZrO_2, TiO_2, and P_2O_5 and their effects have been reported [13–15]. Among these systems, $Li_2O–Al_2O_3–SiO_2$ glass-ceramic, due to its low coefficient of thermal expansion (CTE) [16], could match silicon wafer well and has attracted our attention. We thus studied the influence of ZrO_2 and TiO_2 on microstructures and properties of LAS, and obtained low CTE of $2.56–2.68 \times 10^{-6}$/°C and high flexural strength of 151–157 MPa [14,17].

Some researchers investigated the nucleation effect of Cr_2O_3 in other systems, e.g. $CaO-MgO-Al_2O_3-SiO_2$ glass and found that Cr_2O_3 was a very effective additive for controlling the rate of nucleation [18–20]. However, the effect of Cr_2O_3 on LAS glass-ceramic has not been reported until now. Accordingly, the motive of this paper is to explore the influence and mechanism of Cr_2O_3 addition on the crystallization and properties of LAS system, and further improve the mechanical property.

2. Experimental procedures

The chemical compositions of the $Li_2O–Al_2O_3–SiO_2$ glass-ceramic were listed in Table 1, and reagent grade $Li(OH)\cdot H_2O$, Al_2O_3, H_3SiO_3, ZnO, $Mg(OH)_2$, $Ca(OH)_2$, Cr_2O_3, $Zr(OH)_4$, and H_3BO_3 with purity > 99% were chosen as the raw materials. LAS glass–ceramic in this work was prepared by the melting method as follow. After weighed accurately, the raw materials were ball milled uniformly, and melted in a platinum crucible by an electric furnace

* Corresponding author. School of Microelectronics and Solid-State Electronics, University of Electronic Science and Technology of China, Chengdu 610054, China.
E-mail address: boli@uestc.edu.cn (B. Li).

http://dx.doi.org/10.1016/j.jallcom.2016.09.043
0925-8388/

Table 1
Compositions of $Li_2O–Al_2O_3–SiO_2$ glass-ceramic (wt%).

	Li_2O	Al_2O_3	SiO_2	ZnO + MgO + CaO	B_2O_3	ZrO_2	Cr_2O_3
C1	4	15	58	14	5	4	1
C2	4	15	58	14	5	4	2
C3	4	15	58	14	5	4	3
C4	4	15	58	14	5	4	4

at 1500 °C for 2 h. The molten glass was immediately quenched into distilled water to form cullet. The cullet was grinded using alumina ball and deionized water in the alumina jar for 0.5 h. After dried at 100 °C, the obtained powders added different amount of Cr_2O_3 were mixed by ball milling with deionized water for 7 h. Then, the dry powders prepared above were granulated after mixing with 5 wt% acrylic emulsion, and then uniaxially pressed under a pressure of 25 MPa to obtain the green disks (Φ25 mm × 1 mm) and bars (50 mm × 4 mm × 3 mm). Finally, these compacts were burn out the binder at 450 °C for 3 h, and then sintered in air at 800 °C for 0.5 h.

To analyze the thermal reaction procedure of glass powders and to calculate the crystallization kinetic parameters, the differential scanning calorimeter (DSC, Netzsch STA 449C, Germany) was performed at the heating rates of 5, 10, 15, and 20 °C/min from 20 to 1100 °C in air. The thermal expansion behavior and the coefficient of thermal expansion (CTE) were measured using a dilatometer (Netzsch DIL 402 PC, Germany) at a heating rate of 5 °C/min from 20 to 600 °C. The bulk density of the sintered samples was examined by a precision density balance (And GF-300D, Japan) based on Archimedes method. The dielectric constant and dielectric loss were tested at 1 MHz using a precision LCR meter (Agilent 4284A, USA). The flexural strength was determined by an electromechanical universal testing machine (MTS CMT6104, China). Microstructures of the cross-section for glass-ceramic were observed by a scanning electron microscopy (SEM, FEI Inspect F50, USA). X-ray diffractometer (XRD, PANalytical PW3040/60, Netherlands) using Cu-Kα radiation in the 2θ range of 20–80° in steps of 0.02° was employed to detect the crystal phases.

3. Results and discussions

Fig. 1 show the DSC curves of the four samples obtained at the heating rates of 5, 10, 15 and 20 °C/min. As we know, during the sintering process of $Li_2O–Al_2O_3–SiO_2$, the phase transformation occurs and experiences the following three steps: glass phase → β-quartz solid solution → β-spodumene solid solution → liquid phase. The metastable β-quartz solid solution must develop below 750 °C, and otherwise it will change to β-spodumene solid solution. Additionally, the phase diagram of SiO_2 says the stable β-quartz can form in the temperature range of 230–570 °C, or else it will immediately transform to α-quartz. Therefore, it was considered that an exothermic peak at about 330 °C may be caused by the formation of β-quartz solid solution. The glass transition temperature (T_g) is approximately at 530 °C on the DSC curve. Owing to the crystallization of major phase β-spodumene, a significant exothermic peak is present at around 750–800 °C.

The crystallization peak temperatures (T_p) at different heating rates are marked in Fig. 1 and all the values are listed in Table 2. It can be seen that the values of T_p shift to higher temperatures with increasing the heating rate. Further, the activation energy for crystallization of the glass samples could be decided by using the Kissinger method [21], which is expressed as

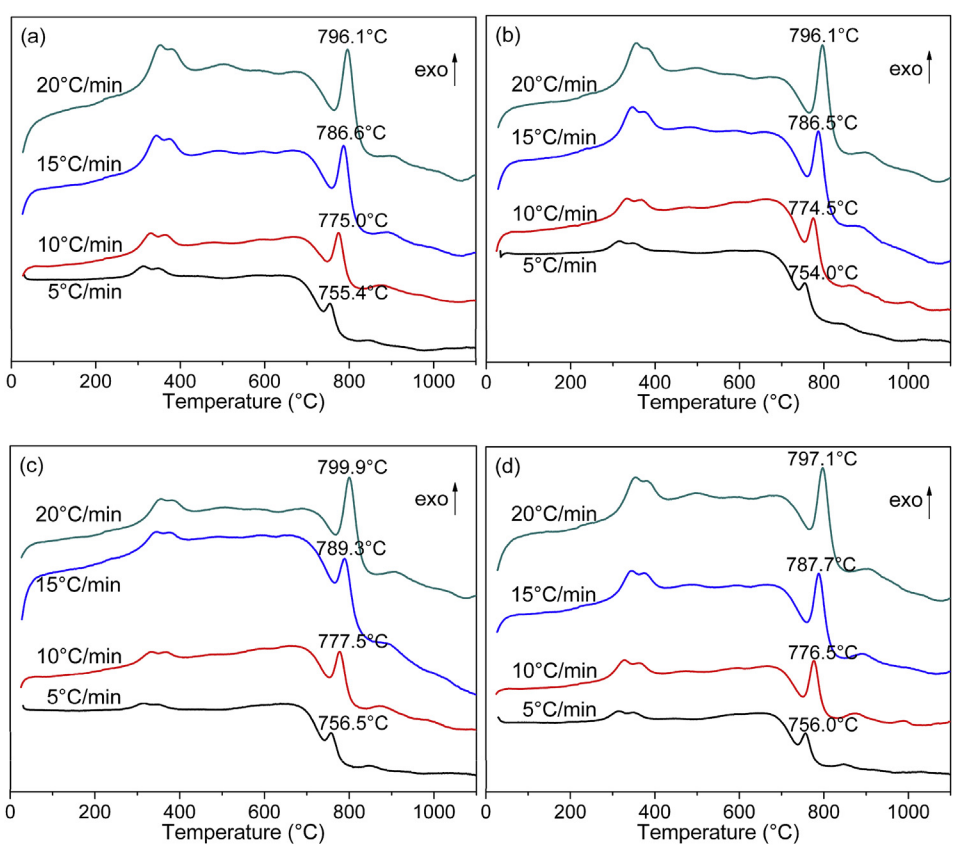

Fig. 1. DSC curves at different heating rates for the glass samples (a) C1, (b) C2, (c) C3, (d) C4.

Table 2
Tp values from DSC curves of LAS glass at different heating rates (°C).

Heating rates (°C/min)	C1	C2	C3	C4
5	755.4	754.0	756.5	756.0
10	775.0	774.5	777.5	776.5
15	786.5	786.5	789.3	787.7
20	796.1	796.1	799.9	797.1

$$\ln\left(T_p^2/\beta\right) = \frac{E}{RT_p} + C \quad (1)$$

where β is the heating rate, E is the activation energy for crystallization, R is the gas constant, and C is constant. Values of E can be calculated using Eq. (1) by plots of $\ln(T_p^2/\beta)$ versus $1/T_p$ which are shown in Fig. 2, and the results are given in Table 3. As we know, the activation energy E is corresponding to the energy barrier of transition from glass to crystal. With more Cr_2O_3 addition, the activation energy E decreases from 158.5 to 149.3 kJ/mol. Specimen C3 has the lowest E value of 149.3 kJ/mol, which means that the glass crystallization become easiest with 3 wt% Cr_2O_3 addition. It is suggested that a proper amount of Cr_2O_3 is beneficial to the crystallization, which is also consistent with the calculation of crystallinity.

The value of crystallization index n can be determined from the Ozawa equation [22].

$$\frac{d[-\ln(1-x)]}{d\ln\beta} = -n \quad (2)$$

where x is the volume fraction crystallized at a fixed temperature T for the heating rate of β. In other words, x is the ratio of the partial area at a given temperature T to the total area under the crystallization exotherm, and its value can be estimated from the exotherms in Fig. 1. The plot of ln [-ln(1-x)] versus lnβ should be a straight line whose slope is n.

Table 3
E and n values of LAS samples.

Crystallization parameter	C1	C2	C3	C4
E (kJ/mol)	158.5	152.1	149.3	156.9
n	4.46	4.69	5.09	4.50

Fig. 3 is Ozawa plots ln[-ln(1-x)] versus lnβ for the glass samples related to exothermic peak shown in Fig. 1. The calculations of crystallization index n are listed in Table 3. The values of n determined from the slopes of these plots vary between 4.46 and 5.09. It is well known that the crystallization index is related to crystallization manner: n = 1, surface crystallization, n = 2, two dimension crystallization, n ≥ 3, volumetric crystallization. Thus, the crystallization index n is more than 3 in this work, indicating that the crystallization manner of samples is the volumetric crystallization.

XRD patterns of LAS with various Cr_2O_3 content sintered at 800 °C are illustrated in Fig. 4. Obviously, $Li_2OAl_2O_37\cdot5SiO_2$ (JCPDS No. 53-1278) is the major phase. The secondary phase is $CaMgSi_2O_6$ (JCPDS No. 83-1817) and the third is ZrO_2 (JCPDS No. 79-1768), which was directly proved by the following calculation. When Cr_2O_3 content ≥2 wt%, some diffraction lines belonging to the new crystal phase Cr_2O_3 (JCPDS No. 82-1484) were found in samples C2-C4. Further, the phase content and the crystallinity of LAS glass-ceramic were estimated by the whole pattern fitting (WPF) method using MDI Jade 6.5. As listed in Table 4, all samples doped with Cr_2O_3 possessed higher crystallinity than 80%, which was elevated from 81.43% to 86.80% by increasing Cr_2O_3 content. This suggested that Cr_2O_3 addition could promote the crystallization of LAS glass. Moreover, the Cr_2O_3 addition could decrease the content of major phase $Li_2OAl_2O_37\cdot5SiO_2$, but increase that of secondary phase $CaMgSi_2O_6$. The third phase ZrO_2 scarcely changed its content with varying the Cr_2O_3 addition. Besides, the result shows that most chromium participated in the formation of the minor crystal phase Cr_2O_3.

Fig. 5 shows SEM micrographs for the fractured LAS glass-

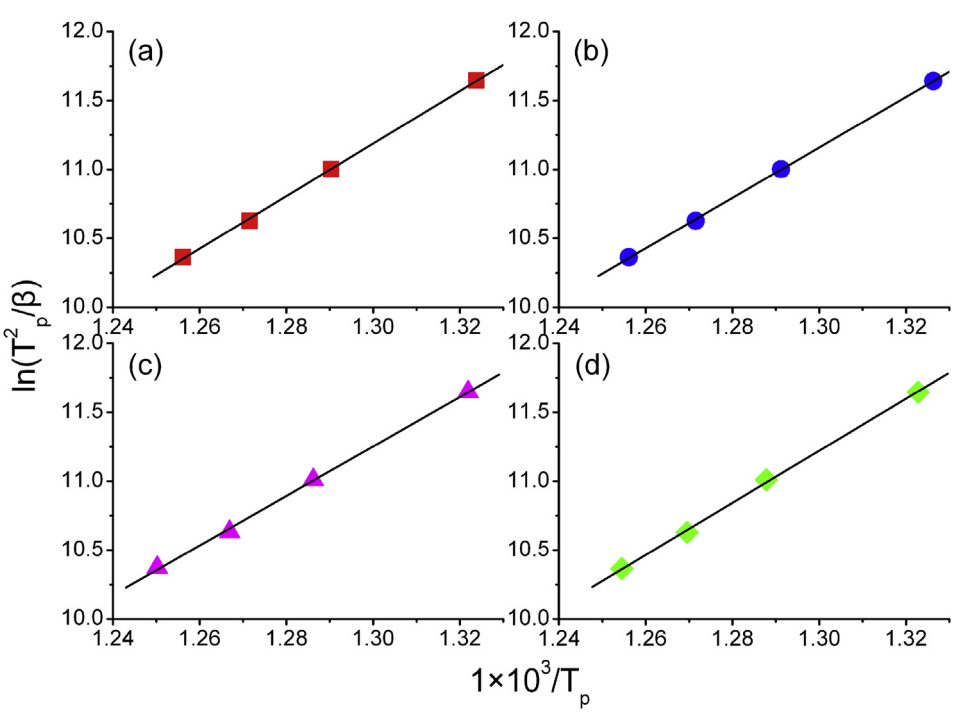

Fig. 2. Relationship between $\ln(T_p^2/\beta)$ and $1/T_p$ for the glass samples (a) C1, (b) C2, (c) C3, (d) C4.

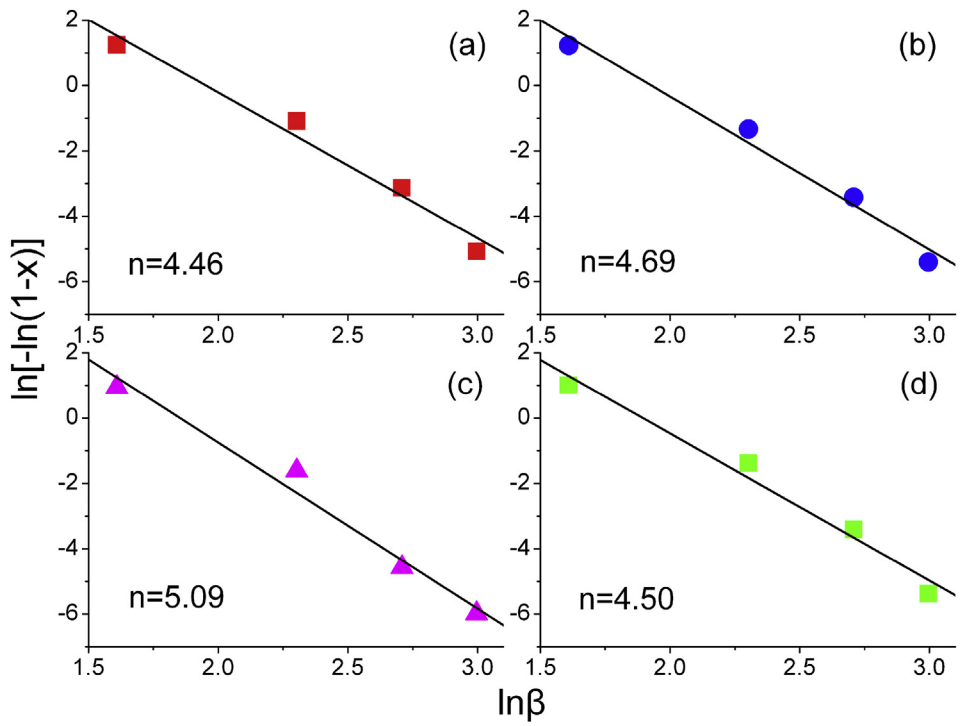

Fig. 3. Relationship between ln[-ln(1-x)] and lnβ for the glass samples (a) C1, (b) C2, (c) C3, (d) C4.

ceramic samples with different amount of Cr_2O_3 sintered at 800 °C. The dense microstructure was formed for all samples doped with Cr_2O_3 and only a few pores were existed inside. The number of pores was gradually reduced with the increase of Cr_2O_3 content. Thus, the sufficient Cr_2O_3 addition could further improve the densification of microstructure for LAS glass-ceramic. Back scattered electron mode was adopted to take SEM images, which allows clear recognition of the formed crystals and the residual glass via different colors. It was observed that the dark gray regions were surrounded by the light gray regions. In order to clarify the constitution of these two regions, EDS analysis was conducted at the corresponding two points on Fig. 5c for sample C3, and the spectra were presented in Fig. 6a and b, respectively. Lithium and Boron, as light elements, cannot be detected by EDS. Both two patterns contained the same elements of Si, Al, Zn, Mg, and Zr. However, the element Cr was not detected in these points, which may result from mainly precipitating as the minor crystal phase Cr_2O_3. It is important to point out that the atomic percentage of Al and Si for point A, in Fig. 6a, is nearly equaled to the major crystal phase $Li_2OAl_2O_37\cdot5SiO_2$. As we known, glass-ceramic is usually composed of the crystal phase as well as the residual glass phase. This demonstrated that the dark gray zone was the major crystal phase $Li_2OAl_2O_37\cdot5SiO_2$ and the light gray zone was the residual glass phase. The small amount of glass phase bonded the crystals together, guaranteeing the mechanical strength. It was clearly seen that the crystals almost exhibited irregular shape and non-uniform size. The crystal size varied in the range of 1–2 μm and the large one reached about 4 μm. The homogeneous dispersion of crystals appeared in the interior of glass-ceramics, indicating that the crystallization mechanism is bulk crystallization. This result is in agreement with the above calculation of crystallization index n. Besides, the widely distributed crystals covered the 80% area of SEM picture, which also verified the crystallinity calculated from XRD analysis.

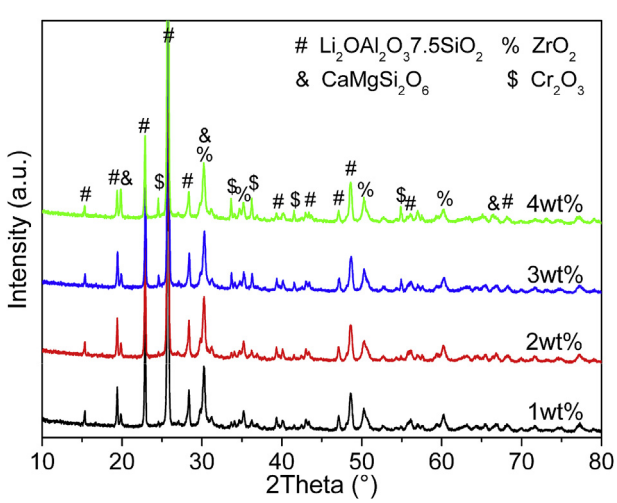

Fig. 4. XRD patterns of LAS glass-ceramics with different Cr_2O_3 content sintered at 800 °C.

Bulk density, shrinkage rate, and mechanical properties of the LAS composites sintered at 800 °C as a function of Cr_2O_3 content are illustrated in Fig. 7. All sintered samples at 800 °C could obtain the higher bulk density than 2.5 g/cm^3 and form the dense microstructure (in Fig. 5), and the change in density is not significant as a

Table 4
Phase content and crystallinity calculated from XRD.

Sample	Phase content (wt%)				Crystallinity (%)
	$Li_2OAl_2O_37\cdot5SiO_2$	$CaMgSi_2O_6$	ZrO_2	Cr_2O_3	
C1	85.5	11.7	2.8	0	81.43
C2	82.1	13.6	2.9	1.4	83.50
C3	80.8	14.1	2.8	2.3	86.80
C4	79.5	14.4	3.0	3.1	84.68

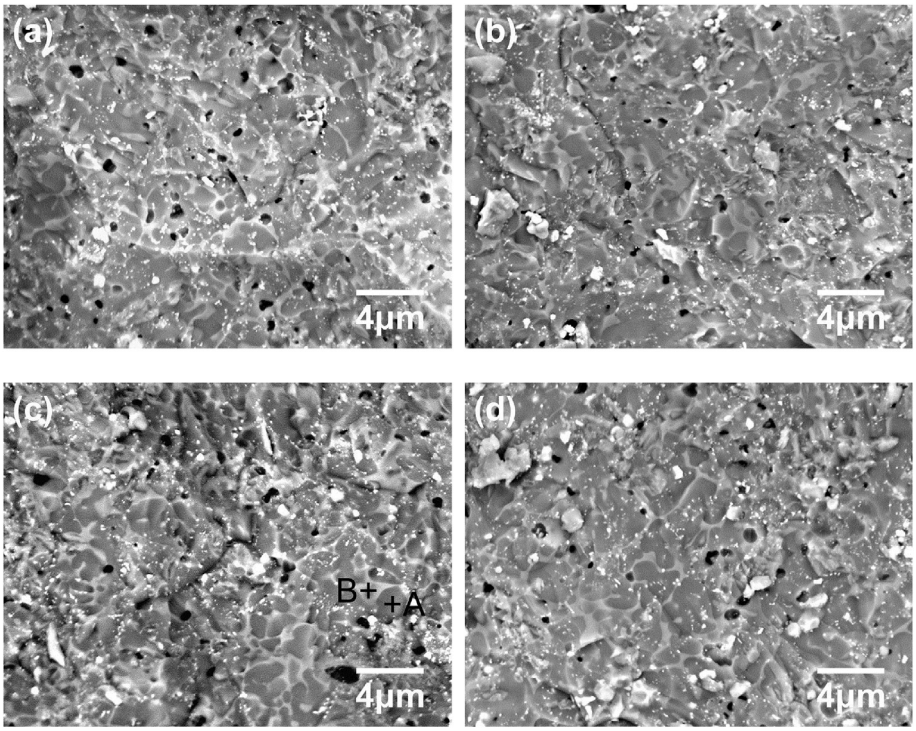

Fig. 5. SEM photographs for fractured samples with different Cr_2O_3 contents sintered at 800 °C for 2 h (a) 1, (b) 2, (c) 3, (d) 4 wt%.

function of Cr_2O_3 content. Nevertheless, the density slightly increased from 2.66 to 2.719 g/cm^3 with increasing Cr_2O_3, which was consistent with the observation of SEM. In addition, the change of shrinkage rate exhibited the same trend as the bulk density, and all samples had higher shrinkage rate than15%, suggesting that the introduction of Cr_2O_3 is helpful for the densification of this system.

As shown in Fig. 7, similarly, the flexural strength of LAS glass-ceramics was significantly enhanced from 140 MPa to 208 MPa, when Cr_2O_3 content increased from 1 to 3 wt%. The reasons must be including two sides. On the one hand, SEM images combined with bulk densities indicated that the increase of Cr_2O_3 could improve the densification of microstructure. On the other hand, we previously found that the mechanical property enhanced markedly when the high thermal expansion phases generated in the glass-ceramic system with low CTE [17]. Accordingly, the enhancement of flexural strength in this work was ascribed to the precipitation of crystal phases, $CaMgSi_2O_6$ and Cr_2O_3, with high CTE values in the LAS system. Unfortunately, excessive Cr_2O_3 will result in the decline of flexural strength, which may be attributed to the decrease of CTE for sample C4.

Fig. 8 depicts the coefficient of thermal expansion (CTE) of LAS

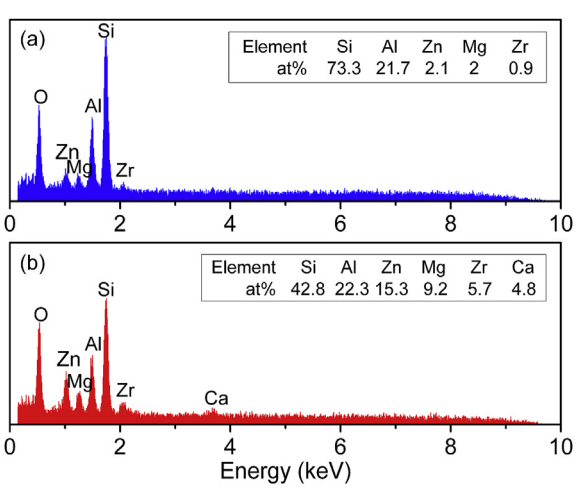

Fig. 6. EDS analysis of sample C3 sintered at 800 °C (a) Spot A, (b) Spot B in Fig. 5c.

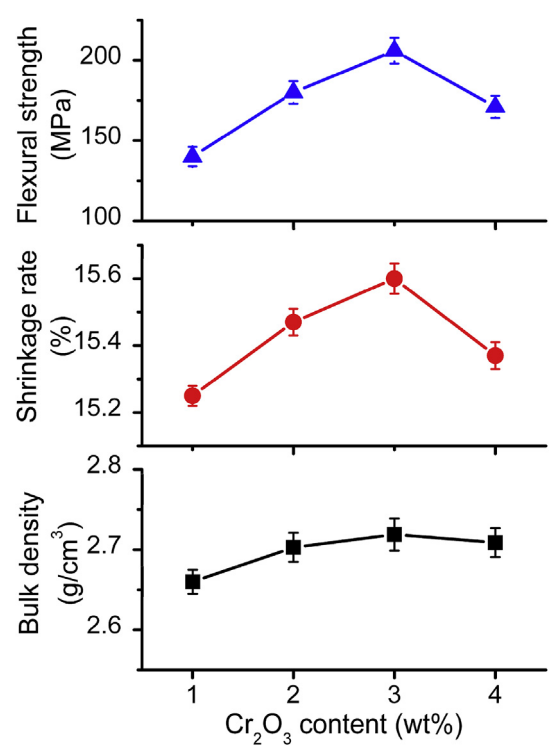

Fig. 7. Bulk density, shrinkage rate, and mechanical properties of the LAS composites sintered at 800 °C as a function of Cr_2O_3 content.

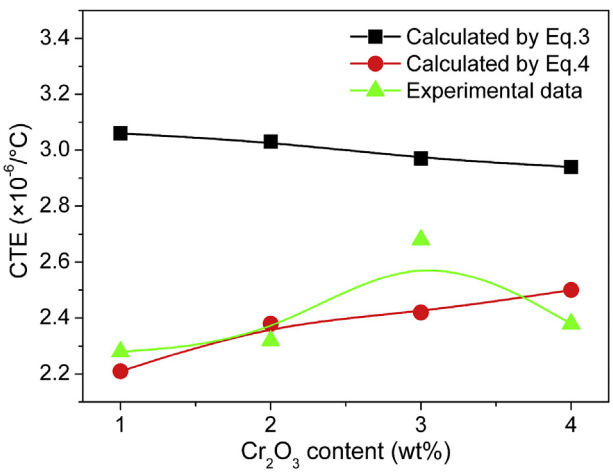

Fig. 8. Calculated and experimental values of CTE versus Cr_2O_3 content.

glass-ceramic versus Cr_2O_3 addition. The value of CTE increased gradually until reaching the maximum (2.68×10^{-6}/°C) for sample C3. It is well known that CTE of glass-ceramic chiefly depended on the components of glass and crystal phases as well as their volume fractions. From the results of XRD analysis in Fig. 4, the increase of Cr_2O_3 promoted the precipitation of crystal phases with high CTE values, that is, $CaMgSi_2O_6$ of 8.25–8.5×10^{-6}/°C [23] and Cr_2O_3 of 7×10^{-6}/°C. But the major crystal phase of LAS glass-ceramic is β-spodumene, having an extremely low CTE value of 0.9×10^{-6}/°C [24]. As a result, sample C3 possesses an expected CTE value of 2.68×10^{-6}/°C, which is close to silicon (3.1×10^{-6}/°C). Usually, Yang et al. [11] calculated the thermal expansion coefficient of glass by the following formula

$$\alpha = \sum x_i \alpha_i \tag{3}$$

where α is the CTE of the desired glass, and x_i and α_i are the mole fraction and CTE value of the oxide species, respectively. CTE of oxides used here are given below: $\alpha(CaO) = 13 \times 10^{-6}$/°C, $\alpha(B_2O_3) = -4.07 \times 10^{-6}$/°C, $\alpha(SiO_2) = 3.72 \times 10^{-6}$/°C, $\alpha(ZnO) = 5 \times 10^{-6}$/°C, $\alpha(ZrO_2) = -10 \times 10^{-6}$/°C, $\alpha(Li_2O) = 26 \times 10^{-6}$/°C, $\alpha(Al_2O_3) = -4 \times 10^{-6}$/°C, $\alpha(MgO) = 6 \times 10^{-6}$/°C, $\alpha(Cr_2O_3) = -0.15 \times 10^{-6}$/°C. However, the calculated CTE values using Eq. (3) are much greater than the experimental data, as shown in Fig. 8. Therefore, we modified the above formula as below

$$\alpha = x_g\alpha_g + x_{c1}\alpha_{c1} + x_{c2}\alpha_{c2} + \cdots \tag{4}$$

where α is the CTE of the glass-ceramic, α_g, α_{c1}, α_{c2}, …represent the CTE value of residual glass phase and each crystal phase respectively, x_g, x_{c1}, x_{c2}, …are the mass fraction of residual glass phase and each crystal phase. In this equation, α_g of residual glass phase is calculated by Eq. (3). x_g, x_{c1}, x_{c2}, …are estimated using the WPF method in Table 4. CTE of crystal phases in this study are given below: α(β-spodumene) = 0.9×10^{-6}/°C, $\alpha(CaMgSi_2O_6) = 8.25 \times 10^{-6}$/°C, $\alpha(ZrO_2) = 10 \times 10^{-6}$/°C, $\alpha(Cr_2O_3) = 7 \times 10^{-6}$/°C. As shown in Fig. 8, the calculated CTE values using Eq. (4) are close to the experimental data, compared with the former results via Eq. (3). Basically, our calculation results are in the acceptable range. Thus, the modified formula Eq. (4) in this work can be used to calculate and predict the CTE for other glass-ceramic systems.

Electrical properties of LAS samples sintered at 800 °C are listed in Table 5. It was found that with increasing Cr_2O_3 content, the dielectric constant (ε_r) and loss (tanδ) increases slightly from 8.1 to 8.5 and 3.25 to 4.4×10^{-3}, respectively. Moreover, the insulation resistivity (ρ) of all samples is more than 10^{12} Ω cm. The increase in dielectric constant and loss may be related to the precipitation of crystal phases. An appropriate amount of Cr_2O_3 did not deteriorate the dielectric properties of LAS glass-ceramic. Sample C3 (3 wt% Cr_2O_3) had good electrical performances: $\varepsilon_r = 8.5$, $\tan\delta = 3.6 \times 10^{-3}$, $\rho = 8.28 \times 10^{12}$ Ω cm, satisfying the requirement of packaging materials.

In addition, the comparison between the commercial LTCC materials and the LAS glass-ceramics in this work was given in Table 6. Obviously, the LAS glass-ceramic we prepared could simultaneously exhibit high flexural strength, low thermal expansion, and good electrical properties, indicating its great potential for packaging in the microelectronic application.

4. Conclusions

To achieve high flexural strength and low thermal expansion, Cr_2O_3 was introduced into Li_2O–Al_2O_3–SiO_2 (LAS) based glass-ceramic. The investigation showed that Cr_2O_3 addition had strong influences on the crystallization, microstructure, as well as the mechanical, thermal, and electrical properties of this material. The increase of Cr_2O_3 content is favorable for decreasing the crystallization activation energies and promoting the crystallization of LAS compounds to form the desired glass-ceramics. XRD analysis identified that the crystalline phases were $Li_2OAl_2O_37 \cdot 5SiO_2$ (major) $CaMgSi_2O_6$, and ZrO_2 (minor). Cr_2O_3 addition could promote

Table 5
Electrical properties of LAS samples sintered at 800 °C.

	C1	C2	C3	C4
Dielectric constant (ε_r)	8.1	8.3	8.3	8.5
Dielectric loss (tanδ)	3.25×10^{-3}	3.30×10^{-3}	3.60×10^{-3}	4.40×10^{-3}
Insulation resistivity (Ω·cm)	3.01×10^{13}	2.02×10^{13}	8.28×10^{12}	2.83×10^{12}

Table 6
Properties of relative commercial LTCC materials [1].

Properties	Ferro A6	DuPont 951	Heraeus CT700	This work
Sintering temperature (°C)	<900	<900	<900	800
Dielectric constant	5.9	7.8	7.0	8.3
Dielectric loss ($\times 10^{-3}$)	2 (10 MHz)	1.5 (1 kHz)	2 (1 kHz)	3.6 (1 MHz)
CTE ($\times 10^{-6}$/°C)	7.0	5.8	6.7	2.64
Flexural strength (MPa)	130	320	240	208

the crystallization of $CaMgSi_2O_6$ and Cr_2O_3 with large CTE value, and thus the thermal expansion and the flexural strength increased with more Cr_2O_3 content. LAS glass-ceramic with 3 wt% Cr_2O_3 sintering at 800 °C exhibited the good performances: high flexural strength (208 MPa), low CTE value (2.64×10^{-6}/°C), low dielectric constant (8.3) and loss (3.6×10^{-3}).

References

[1] M.T. Sebastian, H. Jantunen, Low loss dielectric materials for LTCC applications, Int. Mater. Rev. 53 (2) (2008) 57–90.
[2] D. Nowak, A. Dziedzic, LTCC package for high temperature applications, Microelectron. Reliab 51 (7) (2011) 1241–1244.
[3] K.I. Kim, J.M. Kim, Packaging for RF MEMS devices using LTCC substrate and BCB adhesive layer, J. Micromech. Microeng 16 (1) (2006) 150–156.
[4] K.-H. Chin, C.-C. Chang, C.-H. Chen, LTCC multilayered substrate-integrated waveguide filter with enhanced frequency selectivity for system-in-package applications, IEEE. Trans. Compon. Pack. Technol. 4 (2014) 664–672.
[5] R. Wang, J. Zhou, B. Li, L. Li, CaF_2-AlF_3-SiO_2 glass-ceramic with low dielectric constant for LTCC application, J. Alloys. Compd. 490 (2010) 204–207.
[6] X.Y. Chen, W.J. Zhang, S.X. Bai, Y.G. Du, Densification and characterization of SiO_2–B_2O_3–CaO–MgO glass/Al_2O_3 composites for LTCC application, Ceram. Int. 39 (6) (2013) 6355–6361.
[7] G.H. Chen, L.J. Tang, J. Cheng, M.H. Jiang, Synthesis and characterization of CBS glass/ceramic composites for LTCC application, J. Alloys. Compd. 478 (2009) 858–862.
[8] B.K. Choi, S.W. Jang, E.S. Kim, Dependence of microwave dielectric properties on crystallization Behaviour of $CaMgSi_2O_6$ glass-ceramics, Mater. Res. Bull. 67 (2015) 234–238.
[9] B. Li, Z. Qing, Y. Li, H. Li, S. Zhang, Effect of CaO content on structure and properties of low temperature co-fired glass–ceramic in the Li_2O–Al_2O_3–SiO_2 system, J. Mater. Sci. Mater. Electron 27 (3) (2016) 2455–2459.
[10] S. Wang, H. Zhou, L. Luo, Sintering and crystallization of cordierite glass ceramics for high frequency multilayer chip inductors, Mater. Res. Bull. 38 (2003) 1367–1374.
[11] G. Xia, L. He, D. Yang, Preparation and characterization of CaO–Al_2O_3–SiO_2 glass/fused silica composites for LTCC application, J. Alloys. Compd. 513 (2012) 70–76.
[12] H. Zhu, M. Liu, H. Zhou, L. Li, A. Lv, Study on properties of CaO–SiO_2–B_2O_3 system glass-ceramic, Mater Res. Bull. 42 (2007) 1137–1144.
[13] B. Li, Q. Long, D. Duan, Effects of ZrO_2 on properties of BaO–Al_2O_3–B_2O_3–SiO_2 composites for LTCC applications, J. Mater. Sci. Mater. Electron 27 (2016) 2824–2829.
[14] B. Li, D. Duan, Q. Long, Effects of TiO_2 on microstructures and properties of Li_2O-Al_2O_3-SiO_2 glass-ceramics for LTCC substrates, J. Mater. Sci. Mater. Electron 27 (2016) 7240–7245.
[15] B. Li, Y. Yuan, S. Zhang, Y. Xu, Effects of P_2O_5 on sinterability, microstructures and properties of glass/alumina composites, J. Mater. Sci. Mater. Electron 22 (8) (2011), 924–923.
[16] V.O. Soares, R.C.V.M. Reis, E.D. Zanotto, M.J. Pascual, A. Duran, Non-isothermal sinter-crystallization of jagged Li_2O-Al_2O_3-SiO_2 glass and simulation using a modified form of the Clusters model, J. Non-cryst. Solids 358 (23) (2012) 3234–3242.
[17] B. Li, D. Duan, Q. Long, Influences of ZrO_2 on microstructures and properties of Li_2O–Al_2O_3–SiO_2 glass–ceramics for LTCC applications, J. Mater. Sci. Mater. Electron 27 (1) (2016) 134–139.
[18] L. Barbieri, C. Leonelli, T. Manfredini, G.C. Pellacani, C. Siligardi, E. Tondello, R. Bertoncello, Solubility, reactivity and nucleation effect of Cr_2O_3 in the CaO-MgO-Al_2O_3-SiO_2 glassy system, J. Mater. Sci. Mater. Electron 29 (1994) 6273–6280.
[19] A. Omar, A.W. Elshennauri, G.A. Khater, The role of Cr_2O_3, LiF and their mixtures on crystalline phase formation and microstructure in Ba, Ca, Mg aluminosilicates glass, Br. Ceram. Trans. J. 90 (1991) 179–183.
[20] A. Karamanov, P. Pisciella, M. Pelino, The effect of Cr_2O_3 as a nucleating agent in iron-rich glass-ceramics, J. Eur. Ceram. Soc. 19 (1999) 2641–2645.
[21] H.E. Kissinger, Reaction kinetics in differential thermal analysis, Anal. Chem. 29 (1957) 1702–1706.
[22] T. Ozawa, Kinetic analysis of derivative curves in thermal analysis, J. Therm. Anal. 2 (1970) 301–324.
[23] E.S. Kim, W.J. Yeo, Thermal properties of $CaMgSi_2O_6$ glass–ceramics with Al_2O_3, Ceram. Int. 38 (2012) S547–S550.
[24] O.A. Al-Harbi, Influence of TiO_2 and Cr_2O_3 on crystallinity and properties of Ca, Li aluminosilicate glass, Adv. Appl. Ceram. 106 (2007) 235–240.